

Transport properties of dense deuterium-tritium plasmas

Cong Wang,¹ Yao Long,¹ Xian-Tu He,^{1,2} and Ping Zhang^{1,2,*}

¹*LCP, Institute of Applied Physics and Computational Mathematics,
P.O. Box 8009, Beijing 100088, People's Republic of China*

²*Center for Applied Physics and Technology, Peking University, Beijing 100871, People's Republic of China*

Consistent descriptions of the equation of states, and information about transport coefficients of deuterium-tritium mixture are demonstrated through quantum molecular dynamic (QMD) simulations (up to a density of 600 g/cm³ and a temperature of 10⁴ eV). Diffusion coefficients and viscosity are compared with one component plasma model in different regimes from the strong coupled to the kinetic one. Electronic and radiative transport coefficients, which are compared with models currently used in hydrodynamic simulations of inertial confinement fusion, are evaluated up to 800 eV. The Lorentz number is also discussed from the highly degenerate to the intermediate region.

PACS numbers: 51.30.+i, 51.20.+d, 52.65.Yy

Inertial confinement fusion (ICF) has been a long-desired goal, since the implosion of deuterium-tritium (DT) capsule at reactor-scale facilities is a visible way to generate a virtually unlimited source of energy [1, 2]. In direct-drive ICF, nominally identical Mega-joule-class laser beams illuminate the frozen DT capsule. To trigger the ignition and maximize the thermonuclear energy gain, high compression of the DT fuel and a high temperature of the hot spot should be achieved. In the process of compression, the capsule accelerates and starts to converge since the laser beams ablate DT shell's surface. The DT shell would experience a wide range of thermodynamical conditions at densities up to several hundreds of gram per cubic centimeters (g/cm³) and temperatures from a few to hundreds of electron volts (eV).

Understanding and controlling the high pressure behaviors of DT fuel are of crucial interest for the success of ignition experiments. The equation of states (EOS) of DT fuel are essential for ICF designs, because the low adiabat compressibility of the material is dominated by EOS [3]. During the imploding process, impurities from ablaters or hohlraum are inadvertently mixed into the fuel, which strongly influence the burn efficiency so as the stabilities of plasmas and the mixing rules. Thus, the viscosity and diffusion coefficients of DT mixture are important parameters in hydrodynamic modeling treating interfaces instabilities [4], as well as in further investigating multi-physical effects of high-Z dopants. Finally, accurate knowledge of the electronic and radiative transport coefficients in dense DT plasmas are also important for precisely predicting all kinds of hydrodynamical instabilities grown at the ablation front, at the fuel-ablator interface or at the hot spot-fuel interface, and play central roles to describe the evolution of the central hot spot against the cold fuel [5].

To this end, thermophysical properties of DT mixture are determined by combinations of first-principles molecular dynamics (FPMD) and orbital-free molecular dy-

namics (OFMD) [6, 7] using ABINIT package [8]. Considering DT mixture at high densities, Coulombic pseudopotential with short cutoff radius ($r_{cut} = 0.001$ a.u.) has been built to avoid overlap between pseudocores [9]. As a consequence, large cutoff energy $E_{cut} = 200$ Hartree are used. In this letter, we report QMD calculations for DT mixtures along the 200 to 600 g/cm³ isochore with Γ point to represent the Brillouin zone and 128 particles in a cubic cell, where FPMD and OFMD are performed up to 100 and 10000 eV respectively. Dynamic simulations are lasted from 8000 to 200000 steps in the isokinetic ensemble. Due to the computational limits of finite temperature density-functional theory approach, the electronic structure is calculated up to 800 eV, and a $4 \times 4 \times 4$ Monkhorst-Pack k -point mesh is used. In characterizing the plasma states, the ionic coupling and degeneracy parameters have been used. The definition of the former one is $\Gamma_{ii} = Z^{*2}/(k_B T a)$ (the ratio between the electrostatic potential and the kinetic energy), and the latter one is $\theta = T/T_F$ (the ratio of temperature to Fermi temperature). The present studied plasmas undergoes from strongly coupled ($\Gamma_{ii} \sim 60$) and degenerated states ($\theta \sim 0.01$) to the kinetic states ($\Gamma_{ii} \sim 0.01$ and $\theta \sim 20$).

Concerning the EOS, the difference between FPMD and OFMD lies within 2% accuracy below 20 eV, however, as temperature increases, the difference can be treated as small as negligible. We have constructed the EOS as polynomial expansions (error within 2 %) of the density and temperature ($P = \sum A_{ij} \rho^i T^j$), which can be conveniently used in hydrodynamic simulations in ICF or astrophysics (Table. I). Figure 1 shows the the calculated EOS as a function of temperature at sampled densities. QMD results are compared with both of the ideal and Debye-Hückel models [10]. The pressure of ideal model (P_{id}) can be viewed as the combination of noninteracting classical ions and fermionic electrons. The self-consistent solution of the Poisson equation for a screened charges plasmas leads to the well known Debye-Hückel model, where pressure can be explicitly expressed as: $P_D = P_{id} - \frac{k_B T}{24\pi\lambda_D^3}$. Here, λ_D is the Debye length. At a density of 249.45 g/cm³, the QMD

*Corresponding author; zhang_ping@iapcm.ac.cn

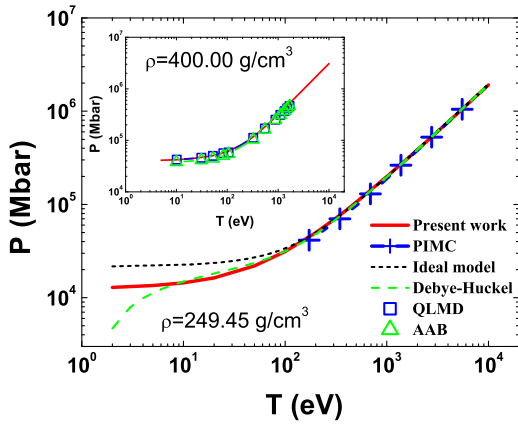


FIG. 1: (Color online) EOS as a function of temperature at 249.45 g/cm^3 (Inset is the EOS for $\rho = 400 \text{ g/cm}^3$). Previous results, including ideal model and Debye-Hückel model, as well as PIMC, QLMD, and AAB numerical simulations, are also shown for comparison.

pressures are 9% \sim 40% smaller than those given by the ideal model, as temperature lies below 100 eV. However, the Debye-Hückel model underestimates the QMD results by 60 %, at the lowest temperature (2 eV) considered. For very high temperatures, beyond T_F , QMD simulation results and the two classical methods merge together into the noninteracting classical ions and electrons (with difference smaller than 1%). Furthermore, good agreement in EOS is achieved between the present results and other simulation methods, such as, Path Integral Monte Carlo (PIMC), Quantum Langevin molecular dynamics (QLMD), and average atom model with energy-level broadening (AAB) [11–13].

TABLE I: Pressure (kbar) expansion coefficients A_{ij} in terms of density (g/cm^3) and temperature (eV).

i	A_{i0}	A_{i1}	A_{i2}
0	671.1939	816.8465	-0.1286
1	12645.2534	753.1419	0.0020
2	151.1943	-0.0401	0.0000

Previous QMD simulations in determining the self-diffusion coefficients and viscosity were limited at low densities (equivalent hydrogen mass density up to 8 g/cm^3) and temperatures (10 eV) [14–17]. The present work substantially extends the study on the transport coefficients into hot dense regime, and comprehensive comparisons with one component plasma (OCP) model are described. Here, the self-diffusion coefficient (D) is derived via particle velocity according to the Green-Kubo relation. The viscosity (η) is computed from the autocorrelation function of the five off-diagonal components of the stress tensor: P_{xy} , P_{yz} , P_{zx} , $(P_{xx} - P_{yy})/2$, and $(P_{yy} - P_{zz})/2$. In order to reduce the length of trajectory, empirical functions $C[1 - \exp(-t/\tau)]$, where C and τ are

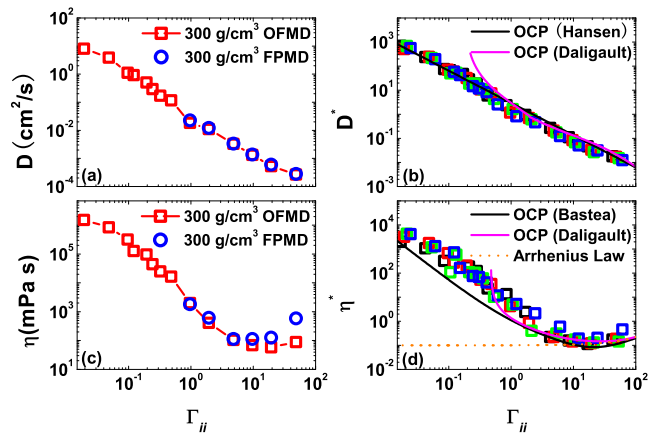


FIG. 2: (Color online) (a) FPMD and OFMD results for the diffusion coefficients; (b) Comparison between OFMD simulations and OCP models for the diffusion coefficients; (c) Viscosity obtained by FPMD and OFMD; (d) Reduced OFMD viscosities are compared with OCP models. For the reduced viscosity and diffusion coefficients, the present OFMD results are denoted by open squares for the density of 200 g/cm^3 (black), 300 g/cm^3 (red), 400 g/cm^3 (green), and 600 g/cm^3 (blue).

free parameters, have been used to fit the integrals of the autocorrelation functions [17]. The fitting procedure is effective in damping the variation and produces reasonable approximations to η (the computed error lies within 10%). Due to the fitting procedure and extrapolation to infinite time, the total error of 20 % has been estimated. The uncertainty in self-diffusion coefficient, where an additional $1/\sqrt{N}$ advantage is secured by particle averages, lies within 2%.

Self-diffusion coefficient and viscosity for DT mixture calculated by FPMD and OFMD as a function of coupling parameter Γ_{ii} at a sampled density of 300 g/cm^3 are shown in the left panels in Fig. 2. As indicated in the figures, FPMD and OFMD results for self-diffusion coefficients are in generally good agreement (error within 5% or better). As for the viscosity, the divergence between FPMD and OFMD could reach up to $\sim 70\%$ at low temperatures, however, as temperature increases, they tend to merge together. In order to compare these results with OCP simulations conveniently, the self-diffusion coefficient D and viscosity η are reduced to a dimensionless form: $D^* = D/\omega_p a^2$, and $\eta^* = \eta/n_i M \omega_p a^2$, where $\omega_p = (4\pi n_i/M)^{1/2} Ze$ is the plasma frequency for ions of mass ($M = 2.5 \text{ amu}$). Memory-function analysis of the velocity autocorrelation function has been used to obtain the diffusion coefficient of OCP ($D^* = 2.95\Gamma^{-1.34}$), however, this result is not accurate at $\Gamma \leq 4$ [18]. Recently, a more accurate fit (valid at $0.5 \leq \Gamma \leq 200$) to the OCP simulations has been provided by Daligault [19]. In Fig. 2 (b), we compare OFMD data with those OCP simulations. The general feature of our simulation result agrees with that of Hansen *et al.* [18], but visible diver-

gence (3% ~ 50 %) is still observed. The accordance of the Daligault's fit with the present results is better at low temperatures. As increasing temperature, the Daligault's OCP fitting overestimates the OFMD results by ~ 40 % at $\Gamma_{ii} = 0.5$. The present results for the reduced viscosity are shown in Fig. 2 (d), where results from OCP simulations are also provided for comparison. By performing classical molecular dynamics of OCP, Bastea [20] fit η^* to the form: $\eta^* = 0.482\Gamma_{ii}^{-2} + 0.629\Gamma_{ii}^{-0.878} + 0.00188\Gamma_{ii}$. The present simulation results for viscosity indicate a similar behavior between dense plasma and normal fluid, that is, both of bodily movement of particles and the action of interparticle forces contribute to the transport of momentum. At large coupling, the viscosity increases with decreasing temperature (or adding density), where an Arrhenius-type relation ($\eta^* = 0.1 \times e^{0.008\Gamma_{ii}}$) is observed. At the intermediate region, $10 \leq \Gamma_{ii} \leq 50$, contributions from the two mechanisms vary with similar magnitude, leading to a shallow minimum. OCP simulations indicate that the minimum lies at around $\Gamma_{ii} = 25$ [19], while our FPMD and OFMD results suggest the minimum near $\Gamma_{ii} = 11$ and $\Gamma_{ii} = 15$, respectively. When $\Gamma_{ii} < 10$, as in a gas, the bodily movement of particles is predominant and, the viscosity increases with temperature.

Apart from the EOS and ionic transport coefficients, the electronic transport coefficients are derived using QMD in the following steps. Ten snapshots are directly taken from FPMD equilibrium trajectories up to 100 eV, however, beyond this value, the structure are extracted from OFMD simulations. Then, the dynamical conductivity $\sigma(\omega) = \sigma_1(\omega) + i\sigma_2(\omega)$ is evaluated through Kubo-Greenwood formula as averages of the selected configurations. The dc conductivity (σ_{dc}) follows from the static limit $\omega \rightarrow 0$ of $\sigma_1(\omega)$. In the Chester-Thellung version [21], the kinetic coefficients \mathcal{L}_{ij} are described as:

$$\mathcal{L}_{ij} = (-1)^{i+j} \int d\epsilon \hat{\sigma}(\epsilon) (\epsilon - \mu)^{(i+j-2)} \left(-\frac{\partial f(\epsilon)}{\partial \epsilon}\right), \quad (1)$$

with $f(\epsilon)$ being the Fermi-Dirac distribution function and μ the chemical potential. The electronic thermal conductivity K_e is given by

$$K_e = \frac{1}{T} (\mathcal{L}_{22} - \frac{\mathcal{L}_{12}^2}{\mathcal{L}_{11}}). \quad (2)$$

The electronic heat conduction as a function of temperature along the isochore of 200 g/cm³ up to 800 eV is shown in Fig. 3 (a). Results from theoretical models, which are currently used in hydrodynamics simulations for ICF, as well as previous *ab initio* simulations, are provided for comparison. Hubbard model [22] is valid for a highly degenerate electron system, where the electronic states are treated by using independent plane waves. The interactions between nuclei are not screened by electrons, and atomic configurations are assumed to be Debye- or OCP-like. Unfortunately, thermal conditions in ICF often enters the partially degenerate regime, which clearly goes beyond the hypothesis

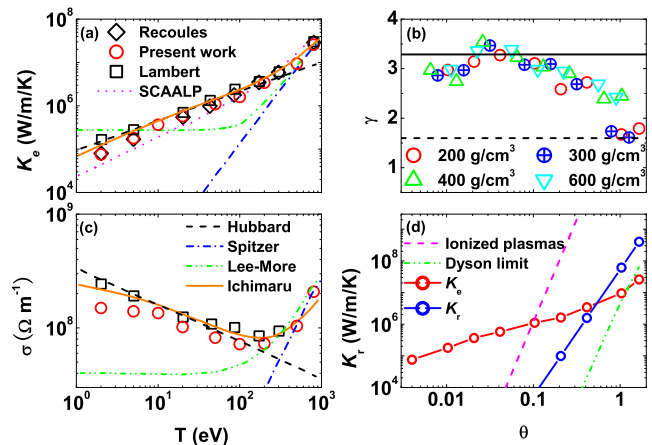


FIG. 3: (Color online) The present results are compared with those of classical models and *ab initio* simulations. (a) Electrical thermal conductivity; (b) Lorentz number; (c) Electrical conductivity; (d) Radiation thermal conductivity. In panels (a) and (c) the labels are combined to present the theoretical and QMD results for K_e and σ_{dc} .

of Hubbard model. Lee-More model [23], which is not quite accurate in the degenerate state, uses different formulas for the electron collision time in solid, liquid, and plasma. The Spitzer model [24], which exhibits a power law on the temperature ($T^{5/2}$), has been dedicated to kinetic plasmas. At high temperatures, our QMD results and Lee-More model merged together into the Spitzer conductivity. From quantum Boltzmann equation coupled with Ziman theory, Ichimaru [25] derived hydrogen transport coefficients restricted to the moderate coupling $\Gamma < 2$. From Fig. 3, clearly, Ichimaru model results overestimate the present data (up to ~ 30%) at the strong coupled regime, and then the difference reduces to 10 %. Remarkably, our QMD data of the electronic thermal conductance for DT mixtures shows reasonable consistency with recent developed self-consistent average-atom model (SCAALP) [26] and precious QMD simulations for hydrogen [5, 7] in a wide range.

Beyond the thermal conductance, the dynamic conductivities are also calculated to examine the Lorenz number defined as:

$$L = \frac{K_e}{\sigma_{dc} T} = \gamma \frac{k_B^2}{e^2}. \quad (3)$$

The nature of the screened potential, which is responsible for the scattering of the electrons, determines γ . L is constant in the degenerate and coupled state (γ is equal to $\pi^2/3$), reducing to the ideal Sommerfeld number. In the nondegenerate case, γ reaches 1.5966 considering e - e collisions. In the intermediate degenerate region, it is difficult to deduce the electronic thermal conductivity from electrical conductance by Wiedemann-Franz law due to the fact that there exists no assumption on the γ value. In Fig. 3 (b) we show the γ value as a function of degeneracy parameter θ for different densities. The simulation

results indicate that the Lorenz number vibrates around the Sommerfeld limit in the degenerate region. As θ increases, the departure of Lorenz ratio from the ideal value towards the lower limit is observed.

Results for σ_{dc} are presented and compared with those obtained by classical models or *ab initio* simulations in Fig. 3 (c). It has been demonstrated that Hubbard model recovered the Wiedemann-Franz law in the degenerate limit, and thus the electrical conductance are computed from the thermal conductance. For the Spitzer model, the electrical conductivity is obtained by using the Lorenz number at the lower limit of kinetic matter including e-e collisions. Our QMD results agree well with Ichimaru model [25] and data by Lambert *et al.* [7] in a wide region between the degenerate state and the kinetic state.

Another useful coefficient, which plays an important role in the energy transport formulation of ICF and astrophysics, is the radiative thermal conductivity (K_r). As usual, it is connected to the Rosseland mean path length ($l_R = \frac{1}{\rho\kappa_R}$ with κ_R the Rosseland mean opacity - RMO) by the following relation [1]:

$$K_r = \frac{16}{3}\sigma_B l_R(\rho, T)T^3, \quad (4)$$

where σ_B is the Stefan-Boltzmann constant. In particular, the RMO can be in the form:

$$\frac{1}{\kappa_R} = \int_0^\infty \frac{B'(\omega)}{\alpha(\omega)} d\omega, \quad (5)$$

where $B'(\omega)$ is the derivative with respect to the temperature of the normalized Planck's function. $\alpha(\omega) = \frac{4\pi}{n(\omega)}\sigma_1(\omega)$ is the absorption coefficient with $n(\omega)$ the real part of the index of refraction. A comparison for K_r is made in Fig. 3 (d) between our QMD simulations and those given by fully ionized plasma and

Dyson limit. Zeldovich and Raizer have proven that [27] the RMO of fully ionized plasma can be obtained as $\kappa_R^{ideal} = 0.014(Z^3/A^2)\rho(k_B T)^{-7/2}$ cm²/g. In this relation, Z is the atomic number, A is the atomic weight, and $k_B T$ is expressed in kilo-eV. The upper limit of RMO ($\kappa_R \leq 6.0 \times 10^3 Z/(A k_B T)$ cm²/g) has been reported by Bernstein and Dyson via applying Schwartz's inequality to a particular factoring of the integrand in the definition of RMO [28]. Our QMD simulation results indicate that K_e governs the energy transport process in the fully degenerate state. As the matter enters the moderate degenerate case, K_r rises about four order of magnitude as the temperature increases from $\sim 10^2$ eV to $\sim 10^3$ eV, and becomes dominant when θ exceeds ~ 0.5 .

In summary, we have determined the EOS and transport coefficients of DT plasmas within QMD simulations in the hot dense regime as reached in future ICF experiments. The wide range EOS has been built from the coupled to the kinetic regime to describe pressures up to 10^6 Mbar. A clear chain of simulations in computing thermophysical properties of hot dense plasma has been demonstrated. The ionic diffusion coefficient and viscosity have been simulated and compared with various OCP model simulations. The electronic and radiative thermal transport coefficients have also been determined, clearly showing different weights when crossing different pressure-temperature regimes. The ability to simulate these parameters in a self-consistent way shown by our results opens a new way to validate classical theoretical models currently used in hydrodynamical simulations for ICF and astrophysics.

This work was supported by NSFC under Grants No. 11005012 and No. 51071032, by the National Basic Security Research Program of China, and by the National High-Tech ICF Committee of China.

-
- [1] S. Atzeni and J. Meyer-ter-Vehn, *The Physics of Inertial Fusion: Beam Plasma Interaction, Hydrodynamics, Hot Dense Matter*, International Series of Monographs on Physics (Clarendon Press, Oxford, 2004).
- [2] J. D. Lindl, *Inertial Confinement Fusion: The Quest for Ignition and Energy Gain Using Indirect Drive*, (Springer-Verlag, New York, 1998).
- [3] S. X. Hu, B. Militzer, V. N. Goncharov, and S. Skupsky, Phys. Rev. Lett. **104** 235003 (2010).
- [4] J. L. Milovich, P. Amendt, M. Marinak, and H. Robey, Phys. Plasmas **11** 1552 (2004).
- [5] V. Recoules, F. Lambert, A. Decoster, B. Canaud, and J. Cl  rouin, Phys. Rev. Lett. **102** 075002 (2009).
- [6] W. Lorenzen, B. Holst, and R. Redmer, Phys. Rev. Lett. **102** 115701 (2009).
- [7] F. Lambert, J. Cl  rouin, and G. Z  erah, Phys. Rev. E **73** 016403 (2006).
- [8] Available at <http://www.abinit.org>.
- [9] C. Wang, X. T. He, and P. Zhang, Phys. Rev. Lett. **106**, 145002 (2011).
- [10] P. Debye and E. H  ckel, Phys. Z. **24**, 185 (1923).
- [11] S. X. Hu, B. Militzer, V. N. Goncharov, and S. Skupsky, Phys. Rev. B **84**, 224109 (2011).
- [12] J.-Y. Dai, Y. Hou, and J.-M. Yuan, Astrophys. J. **721**, 1158 (2010).
- [13] Y. Hou, F. Jin, and J.-M. Yuan, Phys. Plasmas **13**, 093301 (2006).
- [14] I. Kwon, J. D. Kress, and L. A. Collins, Phys. Rev. B **50**, 9118 (1994).
- [15] L. Collins, I. Kwon, J. Kress, N. Troullier, and D. Lynch, Phys. Rev. E **52**, 6202 (1995).
- [16] J. G. Cl  rouin and S. Bernard, Phys. Rev. E **56**, 3534 (1997).
- [17] J. D. Kress, James S. Cohen, D. A. Horner, F. Lambert, and L. A. Collins, Phys. Rev. E **82**, 036404 (2010).
- [18] J. P. Hansen, I. R. McDonald, and E. L. Pollock, Phys.

- Rev. A **11**, 1025 (1975).
- [19] J. Daligault, Phys. Rev. Lett. **96**, 065003 (2006).
 - [20] S. Bastea, Phys. Rev. E **71**, 056405 (2005).
 - [21] G.V. Chester and A. Thellung, Proc. Phys. Soc. (London) **77**, 1005 (1961).
 - [22] W. B. Hubbard, Astrophys. J. **146**, 858 (1966).
 - [23] Y. T. Lee and R. M. More, Phys. Fluids **27**, 1273 (1984).
 - [24] L. Spitzer and R. Härm, Phys. Rev. **89**, 977 (1953).
 - [25] S. Ichimaru and S. Tanaka, Phys. Rev. A **32**, 1790 (1985).
 - [26] G. Faussurier, C. Blancard, P. Cossé, and P. Renaudin, Phys. Plasmas **17**, 052707 (2010).
 - [27] Y. B. Zeldovich and Y. P. Raizer, *Physics of Shock Waves and High Temperature Hydrodynamic Phenomena*. (Academic Press, New York, 1998).
 - [28] B. H. Armstrong, Astrophys. J. **136**, 309 (1962).